International Journal of Applied Earth Observation and Geoinformation 122 (2023) 103394

Contents lists available at ScienceDirect

International Journal of Applied Earth Observation and Geoinformation

journal homepage: www.elsevier.com/locate/jag

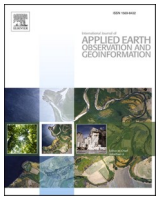

Changes in widespread aquifer properties caused by a magnitude 6-class earthquake evaluated using InSAR analyses

Yutaro Shigemitsu *, Kazuya Ishitsuka, Weiren Lin

Department of Urban Management, Graduate School of Engineering, Kyoto University, Kyoto, Japan
615-8540 C-1-118 Katsura, Kyoto University, Nishikyo-ku, Kyoto City, Kyoto, Japan

ARTICLE INFO

Keywords:
PSInSAR
2018 northern Osaka earthquake
Groundwater level change
Aquifer properties
Correlation coefficient

ABSTRACT

Correlations between surface displacements and groundwater level changes have been widely used to understand aquifer properties and their site characteristics; however, the underlying mechanisms of various correlation types and the influence of earthquakes have not been fully investigated. In this study, we examine correlations between surface displacements from interferometric synthetic aperture radar analyses and groundwater level monitoring data in Osaka and Kyoto, Japan, over 4 years, a period including the 18 June 2018 Mw 5.6 northern Osaka earthquake. Both positive and negative correlations between the seasonal groundwater level changes and the seasonal surface displacements are identified. Based on the observations of the effects of the earthquake, a new conceptual aquifer dynamical model driving the relationship between the surface displacements and the groundwater level changes is proposed. We further reveal that sites with negative correlations increased after the earthquake, suggesting that the earthquake increased the groundwater recharge rate as a result of increases in aquifer transportation properties such as permeability and porosity.

1. Introduction

Natural hazards, such as earthquakes, droughts, floods and typhoons, pose risks to the conservation and management of groundwater resources. In particular, earthquakes cause widespread crustal deformation, altering crustal properties and impacting the quantity and level of the groundwater. Crustal deformation data over a wide area and in time series play an important role in examining areas and the progression of earthquake impacts.

Interferometric synthetic aperture radar (InSAR) is a rapidly advancing geodetic observation technique used to obtain wide-area, time-series surface displacement data. InSAR analyses have spread to a variety of fields, following its initial application to the surface deformation induced by the 1992 Landers earthquake (Wald and Heaton, 1994; Fialko, 2004). Recently, this method has been applied to the estimation of surface displacements caused by groundwater level changes, and many previous studies have revealed permeability or storage coefficients related to correlations between groundwater level changes and surface displacements (Chaussard et al., 2014; Normand and Heggy, 2015; Zhou et al., 2020). Surface displacements can be induced, for example, by earthquake-induced changes in groundwater levels (Ishitsuka et al., 2017; Liu et al., 2018; Ishitsuka et al., 2020). Furthermore, recent studies have shown that surface displacements induced by groundwater level changes prior to an earthquake may serve as earthquake precursors, reflecting subtle alterations in the crustal porosity depending on the crustal stress state (Moro et al., 2017; Wang et al., 2019). Because understanding groundwater behaviour and the nature of aquifers requires intensive knowledge of the overall interactions between groundwater and aquifer skeletons, examining the mechanisms of such correlations, the impact of earthquakes on these correlations and the relationship between earthquakes and aquifer properties is essential.

Seasonal surface displacements caused by seasonal groundwater level changes have attracted attention with respect to understanding the site characteristics of aquifers over wide areas (Castellazzi et al., 2017); such characteristics include the spatial distribution of the skeletal storage coefficient (Chen et al., 2017; Mourad et al., 2021) and the aquifer connectivity (Ishitsuka et al., 2014; Neely et al., 2021). Most previous studies have regarded the correlation between the seasonal surface displacement and the hydraulic head change as a positive relationship (i.e., ground uplift with increasing groundwater level and vice versa). A positive correlation can be explained by the change in the pore pressure

* Corresponding author.
E-mail addresses: shigemitsu.yutaro.76u@st.kyoto-u.ac.jp (Y. Shigemitsu), ishitsuka.kazuya.4w@kyoto-u.ac.jp (K. Ishitsuka), lin@kumst.kyoto-u.ac.jp (W. Lin).

https://doi.org/10.1016/j.jag.2023.103394
Received 31 January 2023; Received in revised form 14 April 2023; Accepted 17 June 2023
Available online 25 June 2023

according to the change in the hydraulic head. However, a recent study by Lu et al. (2020) demonstrated that the correlation can be negative (i.e., ground uplift/subsidence in response to decreasing/increasing groundwater level). In their conceptual model, negative correlations were explained by the cumulative water mass load because an increasing load (i.e., an increase in the hydraulic head) can lead to subsidence (Zhan et al., 2021; Heki and Arief, 2022). The conceptual model implies that whether the correlation is positive or negative could depend on the balances between the influences of the pore pressure and the water mass load (Lu et al., 2020). We speculate that such a variety of groundwater-induced displacement mechanisms may have occurred in many aquifer systems worldwide. However, only a few studies discuss these positive and negative correlations. Moreover, understanding the mechanisms and site characteristics of such contrary types of

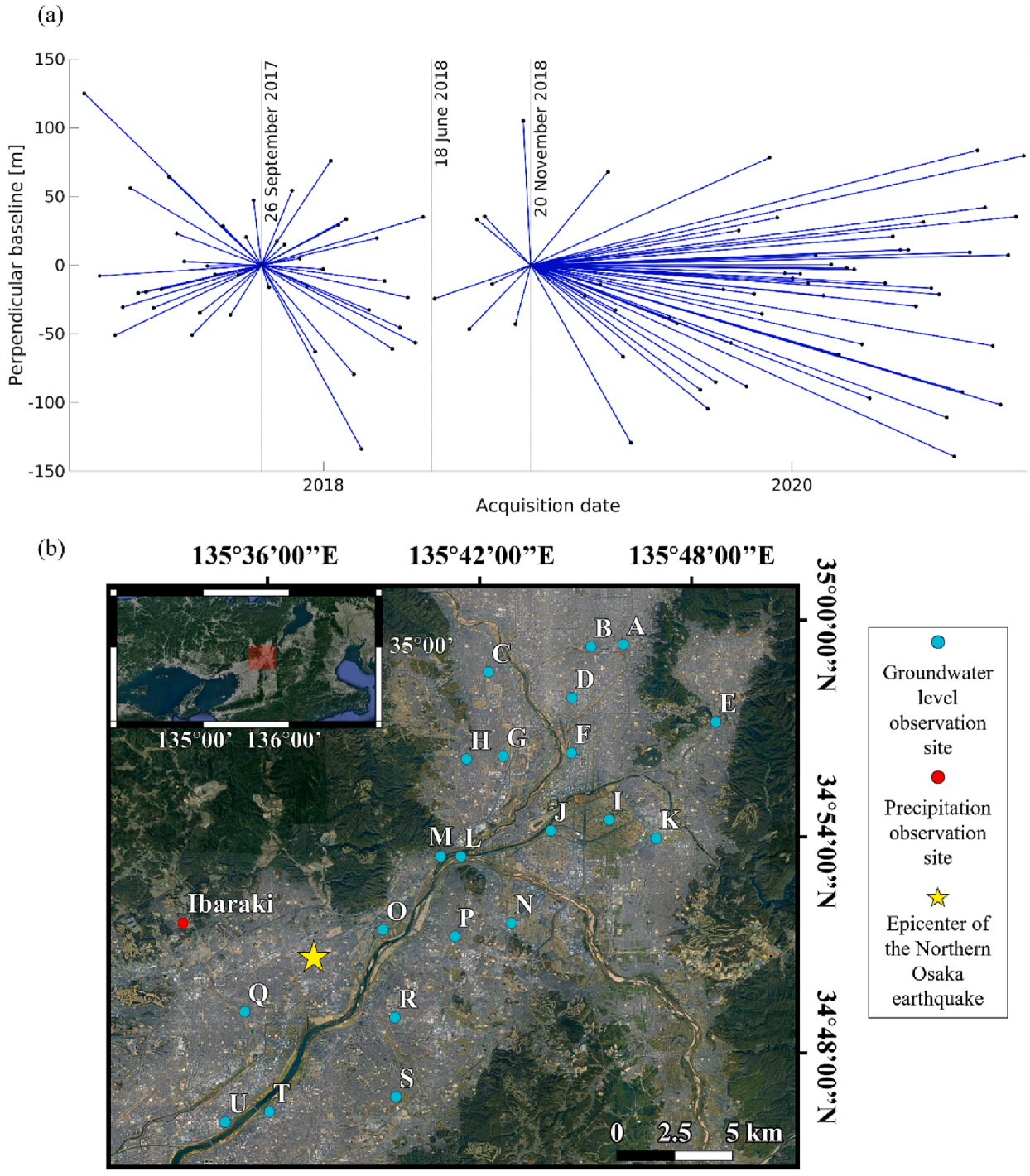

Fig. 1. (a) Combination of Sentinel-1A data used for the interferometric synthetic aperture radar (InSAR) analysis. The date on the horizontal axis is set to the date of the radar irradiations by the satellite in the descending orbit. Data obtained on 26 September 2017 and 20 November 2018 were used as reference data for the InSAR analysis bordering 18 June 2018, when the northern Osaka earthquake occurred. (b) Study area including the Osaka Plain and the Kyoto Basin. The inset shows the Kansai area of Japan, with the red rectangle showing the location of the main map. The groundwater level observation sites are sorted by alphabet from A to U. The background maps were provided by the Environmental Systems Research Institute, Inc. (For interpretation of the references to colour in this figure legend, the reader is referred to the web version of this article.)

correlations is crucial to interpreting InSAR surface displacement data.

Accordingly, this study quantifies the correlation between surface displacements and groundwater level changes using data from 21 groundwater level observation sites from January 2017 to December 2020, including the 18 June 2018 Mw 5.6 northern Osaka earthquake that occurred in the Osaka Plain and Kyoto Basin in Japan (Hirata and Kimura, 2018). Using a surface displacement map from the InSAR analysis and a dense groundwater observation network, we indicate a variety of correlation types in the aquifer system and improve the existing conceptual model to explain these positive and negative correlations. On the basis of this analysis, we illustrate the impact of the Mw 5.6 northern Osaka earthquake, showing changes in the parameters related to the permeability and elastic properties. This might be the first study to find that Mw 6-class earthquakes, which occur frequently worldwide, can change crustal properties over wide areas as well as the seasonal component correlations between the surface displacement and groundwater level changes. In addition, we believe that this finding can contribute to prerequisite knowledge required for groundwater monitoring using InSAR analyses.

2. Methods and target area

2.1. Data

We used synthetic aperture radar (SAR) data obtained from Sentinel-1A, a European Space Agency satellite, to estimate the surface displacements. We analysed a total of 204 orbit scenes, 102 from ascending orbits between 24 December 2016 and 27 December 2020 and 102 from descending orbits between 30 December 2016 and 21 December 2020 (Fig. 1(a) and Table 1). In addition, Global Navigation Satellite System (GNSS) data were used to examine co-seismic and long-term horizontal surface displacements. We used F5 solutions of GEONET coordinates (Hatanaka et al., 2003) recorded from 1 January 2017 to 31 December 2020. The GNSS data were detrended by removing the constant velocity component (i.e., the annual displacement velocity) from the original surface displacement to highlight seasonality trends and co-seismic surface displacement.

Groundwater level data from 1 January 2017 to 31 December 2020 at 21 groundwater level observation sites published by the Water Quality Database were used. Hourly groundwater level data were sampled to convert the data to a daily average. The 21 groundwater level observation sites located near the epicentre of the northern Osaka earthquake were selected (Fig. 1(b) and Table 2). Of these, 15 observation sites are above unconfined aquifers and 6 sites are above confined aquifers. The deeper the strainer mean depth of the observation station, the more likely it is to be classified as a confined aquifer. The maximum depths of the strainers at all the wells were less than 70 m (Table 2).

2.2. Hydrologic characteristics of the analysis areas

The Osaka Plain and Kyoto Basin have abundant subsurface aquifers (Taniguchi and Uemura, 2005). In the Kyoto Basin, the alluvium thickens from the northern part (north of site A in Fig. 1) to the southern part (near site J in Fig. 1). Yoneda et al. (2001) surveyed groundwater properties such as the electric conductivity over the Kyoto Basin, determining the existence of the aquifers from electric conductivity distribution. From the subsurface, loose alluvial sands and soft alluvial clays are deposited in sequence and, deeper down, hard Pleistocene sands and gravels and Pleistocene clays are deposited alternately in a nearly horizontal sequence. In the Osaka Plain, sand and gravel and marine clay layers are alternately deposited from the surface, with unconfined and confined aquifers located above and below the shallowest marine clay layer, respectively (Shintani et al., 2022).

2.3. InSAR analysis methods

The SAR data were analysed using two methods: conventional two-pass differential InSAR (DInSAR) analysis (Massonnet and Feigl, 1998) and persistent scatterer InSAR (PSInSAR) analysis (Kampes 2006). To estimate the daily surface displacements during the 2018 northern Osaka earthquake, a DInSAR analysis and stacking were performed using interferometric pairs of five datasets for the ascending orbits from 30 April to 5 June 2018 and 23 June 2018 and five datasets for the descending orbits from 6 May to 11 June 2018 and 23 June 2018. To estimate the long-term surface displacement, including the co-seismic period, a PSInSAR analysis, which can only extract stable pixels with less noise (Kampes 2006), was performed. A PSInSAR analysis usually assumes a linear constant-velocity model of the surface displacement (Ferretti et al., 2000; Ferretti et al., 2001); accordingly, we followed this assumption here. However, linearity for a duration including an earthquake may not be maintained because of the sudden surface displacement caused by the earthquake. Therefore, we split the primary data into two periods, before and after the earthquake, and separated the InSAR analysis for these two periods (Fig. 1(a)). The annual displacements were then calculated from the estimated time-series displacements using the least squares method. In this paper, the Gamma software was used for the differential interferometric processing (Werner and Strozzi, 2000; Wegnüller et al., 2016) and StaMPS, developed by Stanford University, was used for the phase unwrapping (Hooper and Zebker, 2007; Hooper et al., 2012). To remove atmospheric noise, we performed a temporal filtering (Ferretti et al., 2000), with a moving average of 200 × 200 pixels in the spatial direction and 30 days in the temporal direction. We changed the parameters in the persistent scatterer (PS) candidate selection and PS selection sections to obtain results for a total of six analysis conditions, as shown in the following equations.

$$\widehat{\sigma}_{\phi} = \frac{\sigma_a}{\overline{a}} \tag{1}$$

$$\Gamma = \frac{1}{N}\left|\sum_{n=1}^{N} exp\{j(\phi_{noise})\}\right| \tag{2}$$

Here, $\widehat{\sigma}_{\phi}$ is the amplitude dispersion index (*adx*), σ_a is the standard variance of the amplitude and $\overline{a}$ is the average amplitude of a pixel. ϕ_{noise} denotes the stochastic observation error resulting from the decrease in coherence, and Γ denotes the phase coherence (*coh*). *n* and *N* denote the number of interferometric pairs and the total number of interferometric pairs, respectively. *adx* was tested for two conditions, 0.25 and 0.35, and *coh* was tested for three conditions, 0.60, 0.70 and 0.80 to ensure the robustness of the results around the commonly used thresholds (Ishitsuka et al., 2020). PS pixels are often located at manmade objects in urban areas; therefore, this analysis is suitable for surface displacement estimations in the Osaka Plain and the Kyoto Basin, where major cities (Osaka and Kyoto) are located. The correlation between the surface

Table 1
Data from the European Space Agency Sentinel-1A satellite used in the persistent scatterer interferometric synthetic aperture radar (PSInSAR) analysis.

Satellite	Satellite orbit direction	Data observation period	Number of scenes	Incident angle	Satellite travelling direction angle	Path / Frame	Polarization	Beam mode
Sentinel-1A	Descending	30/12/2016–21/12/2020	102	37-40°	N13°W	17/474	VV	IW
	Ascending	24/12/2016–27/12/2020	102		N193°S	10/107		

Table 2
Symbol, site name and strainer depth of each groundwater level observation site.

Symbols	Site name	Strainer depth (m)			Confined or Unconfined	Latitude (°)	Longitude (°)
		Centre	Min	Max			
A	Hiyoshi	8.1	0.0	16.1	U	34.8190722	135.5891667
B	Toji	59.3	53.3	65.3	C	34.9530556	135.8113889
C	Katsura	14.2	8.2	20.2	U	34.8908333	135.6911111
D	Kamitoba	51.7	45.7	57.7	C	34.9027778	135.7336111
E	Daigo	10.2	8.2	12.2	U	34.9888889	135.7677778
F	Shimotoba	43.2	37.2	49.2	C	34.9641667	135.7436111
G	Kamiueno	9.4	6.9	11.9	U	34.9372222	135.7111111
H	Nagaokakyo	45.2	40.2	50.2	C	34.7797222	135.6605556
I	Oguraike	23.3	10.3	36.3	U	34.9761111	135.7041667
J	Higashiimoarai	43.7	37.2	50.2	C	34.8538889	135.6883333
K	Ogura	8.6	5.9	11.2	U	34.9358333	135.6938889
L	Gokobashi	26.0	22.0	30.0	U	34.8163889	135.6600000
M	Oyamazaki	18.3	15.5	21.0	U	34.8991667	135.7833333
N	Yawataminami	20.2	10.7	29.7	U	34.9077778	135.7611111
O	Takatsuki	10.7	7.2	14.2	U	34.8908333	135.6816667
P	Kuzuha	12.0	9.2	14.7	U	34.7727778	135.6008333
Q	Ayukawa	8.2	7.0	9.4	U	34.9386111	135.7433333
R	Nakamiya	10.2	6.2	14.1	U	34.8569444	135.6544444
S	Kasuga	9.5	4.0	15.0	U	34.9877778	135.7525000
T	Shimeno	26.2	22.2	30.2	U	34.7680556	135.5800000
U	Torikainishi	47.5	41.8	53.2	C	34.8600000	135.7150000

displacements and the groundwater level changes in the target area has been qualitatively pointed out in the past (Hashimoto, 2016). When comparing the obtained surface displacements with changes in the groundwater levels, PS pixels within a 1 km square around each groundwater observation station site were extracted and the average surface displacement value of these PS points was used for the comparison with the groundwater level. In addition, we performed a 2.5-dimensional analysis to calculate the surface displacement in the vertical direction using data from the descending and ascending orbits (Fujiwara et al., 2000).

To quantitatively evaluate the correlations between the surface displacements and the groundwater level changes, we calculated the cross-correlation coefficients (CCCs) using the following equation.

$$R_{xy}(\tau) = \overline{x(t)y(t+\tau)} / \sqrt{\overline{x^2} \bullet \overline{y^2}} \quad (3)$$

Here, R_{xy} is the CCC ($-1 \le R_{xy} \le 1$), x is the groundwater level change, y is the vertical surface displacement,$\overline{x}$ and $\overline{y}$ are the average values, t is time and τ is the time lag. In this study, positive correlations were established for R_{xy} values greater than 0.2, negative correlations were established for R_{xy} values less than −0.2 and no correlations were identified for values between −0.2 and 0.2.

Before calculating the CCC, we applied pre-processing to reduce the linear component. In the first period, we used 11 June 2018 as the reference date, and in the second period, 23 June 2018 was used as the reference date (on the reference date, the surface displacement was set to zero). The data were resampled via spline interpolation to obtain the same number of samples as in the groundwater level change data, and the 10-day moving average was calculated. The data were normalized by the absolute values of the maximum and minimum values when they exceeded 1 mm and −1 mm, respectively. The linear trend representing the long-term trend was then removed to evaluate the seasonal component correlations. The groundwater level change data were similarly processed. The missing data were resampled via spline interpolation, with 18 June 2018 as the reference date, and then the linear trend indicating the long-term trend was removed. High-frequency variations in the groundwater level changes were observed at four sites, D, F, P and T; accordingly, the high-frequency changes were removed by applying a 14-day moving average process. Finally, the data were normalized by the absolute values of the maximum and minimum values when they exceeded 1 m and −1 m, respectively.

Because we calculated the CCCs each year, six correlation coefficients for each condition between January 2017 and December 2020 were obtained at each site. We then calculated the averages and standard deviations of the coefficients for each site.

3. Results

3.1. Co-seismic surface displacements during the 2018 northern Osaka earthquake

Fig. 2(a) and 2(b) shows the daily co-seismic surface displacements in the satellite line-of-sight direction during the 2018 northern Osaka earthquake co-seismic period for the ascending and descending orbits, respectively. The data for the 5 June 2018 ascending was only for the southern half of the range in the image (Fig. 2(a)). Although Fig. 2(a) and 2(b) show phase changes within approximately ± 1 mm/day in terms of surface displacement, considering the accuracy of DInSAR analysis, it is not clear whether these patterns are due to surface displacements or observation errors. However, no significant surface displacement was identified at least around the epicenter of the 2018 northern Osaka earthquake. Fig. 2(c) shows that there were also no significant surface displacements in the horizontal direction before or after the earthquake at the five GNSS stations (see Fig. S1). Therefore, we conclude that no significant surface displacement occurred during the 2018 earthquake.

3.2. Surface displacements and groundwater level changes during the periods before and after the earthquake

The spatial patterns of the surface displacements were similar for the surface displacement maps obtained with the various combinations of the candidate *adx* and *coh* values (see Fig. S2). We use the surface displacement obtained using $adx = 0.25$ and $coh = 0.60$ in the following discussion because this surface displacement pattern resembles most of the surface displacements derived when using other parameter settings. The annual displacement patterns revealed by the Sentinel-1A interferograms differed before and after the earthquake (Fig. 3 and Fig. S2). Data from the period before the earthquake, covering approximately 1.5 years from the end of 2016 until just prior to the earthquake, and data from the period after the 2018 earthquake, covering approximately 2.5 years from immediately after the earthquake until the end of 2020, were utilized. The uplift in the black-framed area in Fig. 3(a) and 3 (b) agrees with the results of a previous InSAR analysis by Morishita

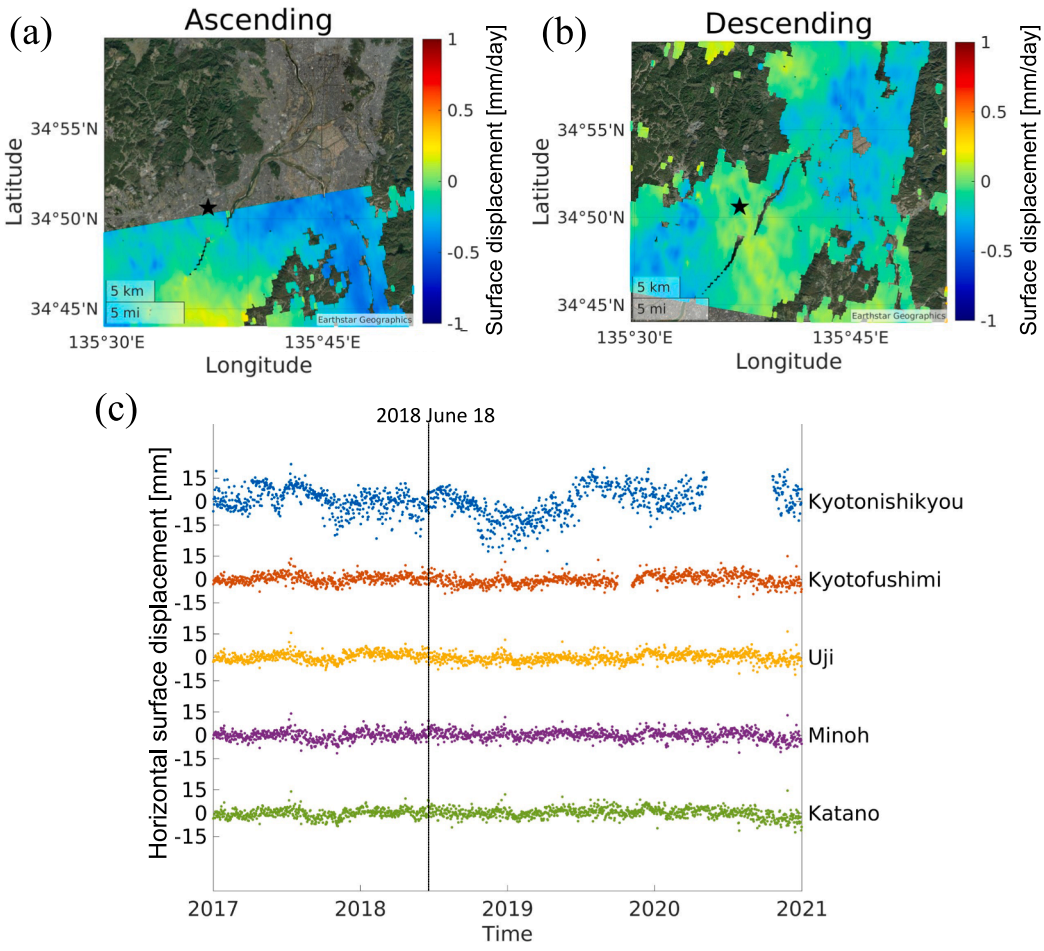

Fig. 2. Surface displacements in the satellite line-of-sight direction according to the InSAR analysis using (a) the five datasets for the ascending orbits from 30 April 2018 to 23 June 2018 and (b) the five datasets for the descending orbits from 6 May 2018 to 23 June 2018. The black star indicates the epicentre of the earthquake. (c) Surface displacements of the horizontal component calculated with positive north and east direction at five GNSS stations from 2017 to 2020 with respect to 1 January 2017.

(2021), and our results further show that the black-framed areas of uplift became even larger after the earthquake. Fig. 4 shows the difference in the annual groundwater level changes before and after the earthquake. After the earthquake, the annual groundwater level dropped in the vicinity of site O and tended to rise in some locations. Comparing the annual groundwater level changes before and after the earthquake, we see that the map patterns of the annual surface displacement after the earthquake (Fig. 3(b)) are generally correlated (Fig. 4(b)). This agreement of the patterns likely indicates that the uplift and subsidence after the 2018 earthquake were associated with groundwater level changes. Conversely, the annual displacement pattern before the earthquake showed only a weak correlation with the groundwater level changes (Fig. 3(a) and Fig. 4(b)).

Comparing the time-series surface displacements and groundwater level changes, we found seasonal component correlations at 18 groundwater level observation sites (Fig. 5; see Fig. S3). The origin of the seasonal component of the groundwater level change could be precipitation, groundwater supply from mountainous areas and/or seasonal artificial extraction. A comparison of the precipitation and groundwater level at site Q (Ayukawa) indicates that the groundwater level rose and fell with increasing and decreasing precipitation (Fig. 6), respectively, suggesting that precipitation was the primary cause of the groundwater level changes at this location. This relationship between the precipitation and the groundwater level change can be observed at nearly all sites, other than sites D, H, N, S and T. Conversely, the groundwater level changes at sites H and N exhibited rapid declines, unlike the temporal pattern of precipitation (Fig. 5c, 5d and 6), implying that other factors such as artificial extraction might have had a significant influence.

We classified the patterns of the seasonal component correlations into three categories: positive correlation (PC), negative correlation (NC) and no correlation (UC). Sites H and N were categorized as PC, showing the ground surface rising and subsiding in correspondence with the groundwater level increases and decreases, respectively (Fig. 5(a) and 5(b)). The UC category was identified at three sites, D, S and T, where the time-series surface displacements were not significantly related to the groundwater level changes (Fig. S3(a) and S3(b) for sites D, S and T). In the other 16 sites belonging to the NC category, we found that the time-series surface displacements and groundwater level changes were negatively correlated. At these sites, the surface subsided despite increases in the groundwater level and the surface rose when the groundwater level fell (Fig. 5(c) and 5(d)).

We found that negative correlations became more significant after the 2018 northern Osaka earthquake because of the larger surface displacements. For example, at sites Q and C, the negative correlations between the time-series surface displacements and the groundwater level changes were not significant prior to the earthquake; however, the correlations became more significant after the 2018 earthquake (Fig. 5 (c) and 5(d)).

Seasonal component correlations are observed around all the groundwater level sites, except at the UC sites, D, S and T. The peaks in the correlations, including both the positive and negative correlations, appear approximately every 365 days (Fig. 7; see Fig. S4). Even though some previous studies have found that the correlation between the time-series displacement and the groundwater level may have a time lag (Normand and Heggy, 2015; Zhou et al., 2020), the time-series data used in this study did not exhibit significant time lags.

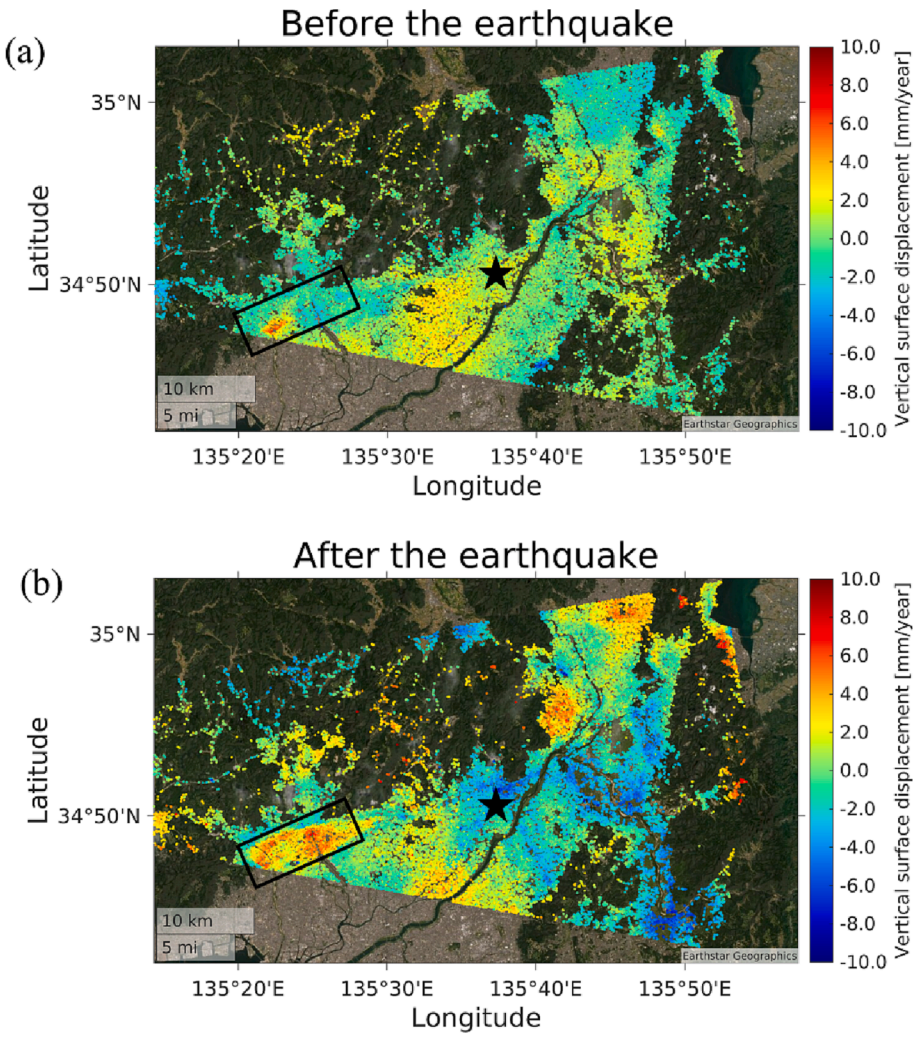

Fig. 3. Annual vertical surface displacements according to the PSInSAR analysis (a) before the earthquake and (b) after the earthquake with $adx = 0.25$ and $coh = 0.60$. The blue colour indicates subsidence displacement, the red colour indicates uplift and the black star indicates the epicentre of the earthquake. (For interpretation of the references to colour in this figure legend, the reader is referred to the web version of this article.)

3.3. Quantification of the correlations between the time-series displacement and the groundwater level

The results of the coefficients for the entire analysed period are shown in Fig. 8(a) and Table S1. The CCC patterns were generally consistent with the qualitative PC, NC and UC classifications described in Section 3.1. Because the orders of the standard deviations were mostly smaller than those of the average, we concluded that the variations in the coefficients for each condition were not large and that the CCC site differences were statistically significant.

3.4. Correlation changes before and after the 2018 northern Osaka earthquake

We calculated the change in the CCCs before and after the 2018 northern Osaka earthquake (Fig. 8(b) and Table S2) by dividing the surface displacement and groundwater level change data into two periods (Fig. 1(a)). Because the standard deviations did not change significantly before and after the earthquake (Table S2), we believe that our evaluation of the CCC changes is valid. One of the main findings of this study is that the CCCs after the earthquake are clearly smaller for all sites except site S. That is, the CCCs shifted from PC before the earthquake to NC after the earthquake. Furthermore, some sites classified as UC before the earthquake shifted to NC after the earthquake (Fig. 8(b)). It is difficult to believe that any event other than the earthquake caused these changes in the correlation during that period; therefore, we interpret the changes in the correlation as being induced by the 2018 northern Osaka earthquake. To the best of our knowledge, such changes in the correlation before and after an earthquake have not been previously reported.

To examine the spatial characteristics of the correlation change, we plotted the distribution of the correlation changes at each site (Fig. 9(a) and 9(b)). The spatial pattern at the groundwater level observation sites indicates that the type of correlation change differed even over short distances (Fig. 9(a) and 9(b)). The spatial pattern implies that the aquifer characteristics are spatially complex and that the aquifer properties may be highly heterogeneous. For example, site H is categorized as PC and site G is categorized as NC (Fig. 9(a) and 9(b)). Compared with a previous study by Lu et al. (2020), our calculations indicate that the correlations between the surface displacements and the groundwater level changes are more spatially dense, therefore demonstrating the effectiveness of InSAR analyses and dense groundwater measurements for classifying the characteristics of aquifers at higher resolution.

4. Discussion

There are four potential causes of the changes in the seasonal groundwater level changes resulting from the earthquake (Ishitsuka

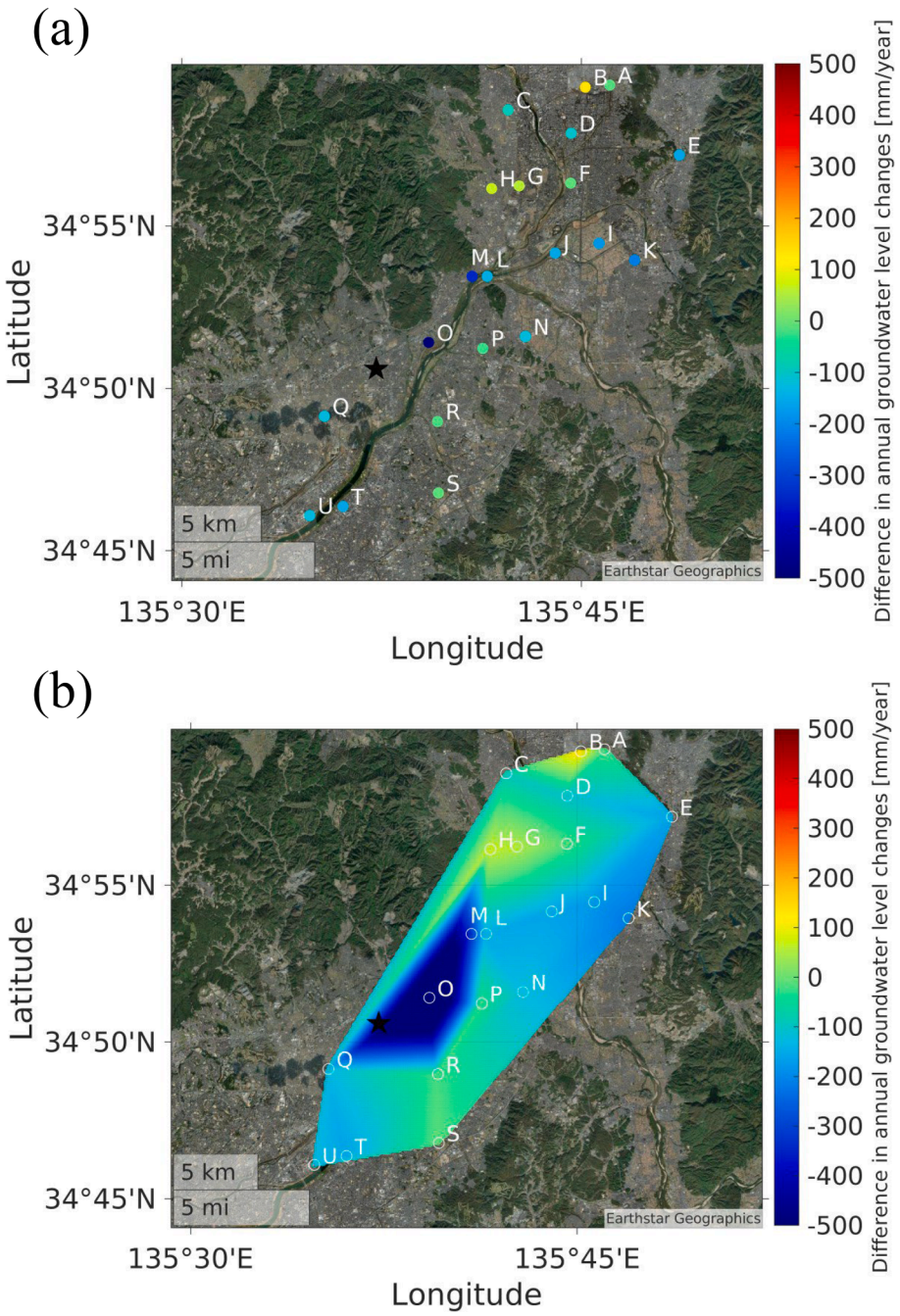

Fig. 4. (a) Difference in the annual groundwater level changes before and after the earthquake at the groundwater level observation sites. (b) Interpolated difference of the values in panel (a) using a two-dimensional linear interpolation based on triangulation. The black star indicates the epicentre of the earthquake.

et al., 2016): (1) groundwater flow resulting from stress changes in the crust (Jónsson et al., 2003); (2) groundwater flow through fractures caused by fault rupture (Hosono et al., 2019); (3) groundwater flow caused by dilation in the ground resulting from fault rupture (Fielding et al., 2009) and (4) groundwater flow in the pore zone caused by seismic waves (Manga et al., 2012; Ishitsuka et al., 2017).

The likelihood of phenomenon (1) is low because the temporal stress changes cannot explain the seasonal displacement patterns observed in this study, which occurred for an extended period (2.5 years) following the earthquake. Phenomena (2) and (3) are expected to lead to an increase in aquifer porosity. Nevertheless, ground water level changes caused by these phenomena would occur only near the fault (~1 km from the fault trace). Because surface displacements were not apparent around the epicentre during the co-seismic and post-seismic periods, it is unlikely that the earthquake-induced groundwater level changes in the Osaka and Kyoto areas were solely due to fault rupture. Phenomenon (4) is the most likely of the four. This phenomenon has been explained by increases in the porosity and permeability of the aquifer, resulting from seismic vibrations, not only along a seismic fault but also across distant areas (Manga et al., 2012). Seismic vibrations mobilize colloids and droplets stuck in pores, resulting in permeability alterations (Manga et al., 2012), and groundwater level changes possibly linked to this phenomenon have frequently been observed with Mw 6-class earthquakes (Manga et al., 2012). In addition, near the area analysed in this study, even though the geology and magnitude of the seismic motion differed, a temporary increase in the permeability was observed on Awaji Island (~60–100 km from the target area in this study) during the 1995 Mw 6.9 Southern Hyogo Prefecture earthquake (Tokunaga 1999).

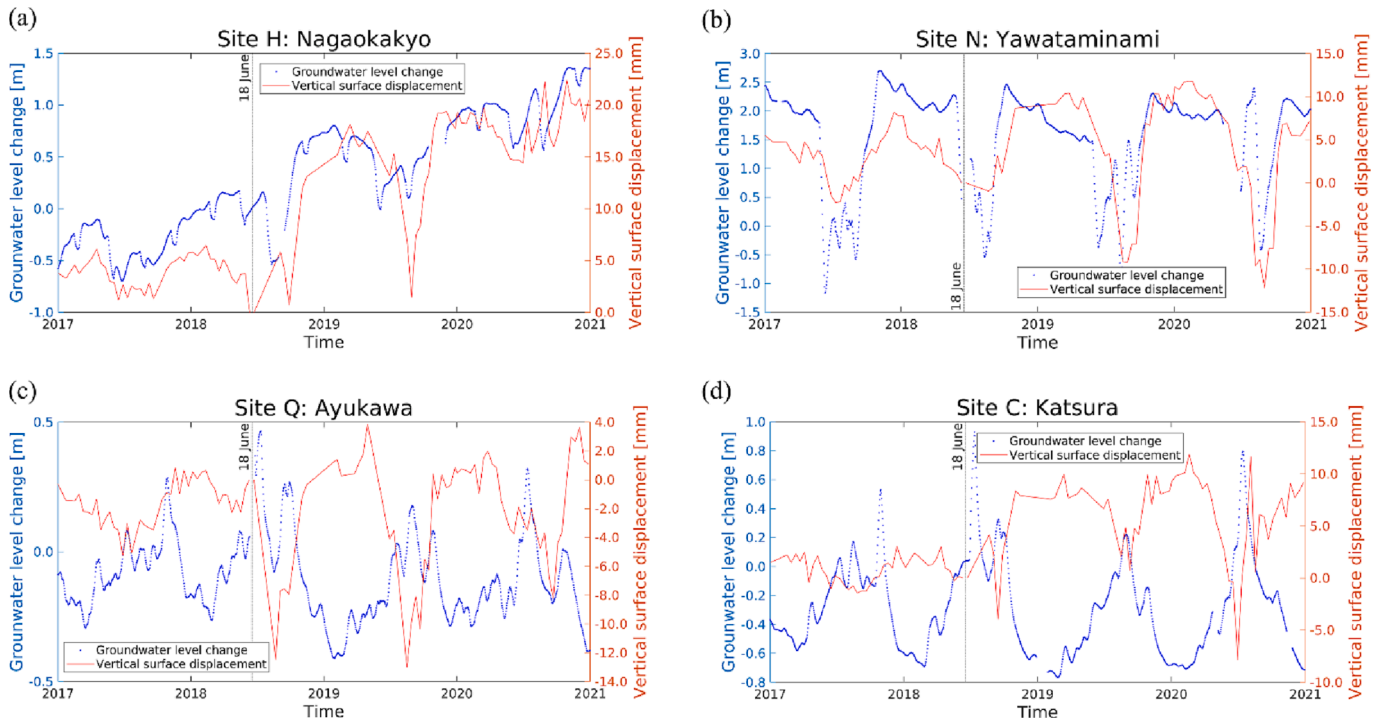

Fig. 5. Comparison of time series of the vertical surface displacements and groundwater level changes at sites H, N, Q and C. The locations of the sites are shown in Fig. 4.

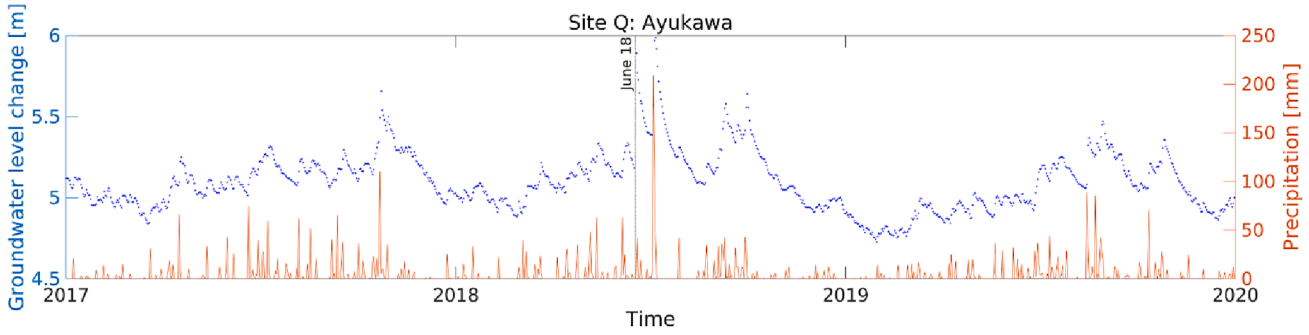

Fig. 6. Example of the seasonal groundwater level change and the amount of precipitation per day. Here, we show the groundwater level change at the Ayukawa groundwater level observation site and the precipitation at the Ibaraki observation site.

Note, however, that the permeability may decrease after an earthquake in some cases.

Fig. 9(c) and 9(d) shows the distribution of the correlation change overlaid on the site amplification factor map from the Japan Seismic Hazard Information Station. The areas with greater amplification factors primarily consist of alluvium and have thicker aquifers (Shintani et al., 2022). In areas with large amplification factors, the negative correlation increased, while no correlation or positive correlations were found in areas with relatively small amplification factors. This indicates that the geological structures related to the seismic amplification were linked to changes in the correlation between the surface displacement and the changes in the groundwater levels during the post-seismic period. In fact, it has been shown that the area of permeability alteration caused by phenomenon (4) increases with increasing earthquake magnitude (Manga et al., 2012). Therefore, the porosity and permeability may have increased in areas where the earthquake shaking was more intense. The possibility of changes in the aquifer transportation properties is further evaluated in Sections 4.1 and 4.2.

4.1. Change in the groundwater response and aquifer properties before and after the earthquake

To investigate whether the groundwater level response to precipitation changed before and after the earthquake, we applied a numerical equation (Park and Parker, 2008) to the daily average groundwater level data at the groundwater level observation site Q in Ayukawa and the daily average precipitation data at the precipitation observation site in Ibaraki (Fig. 1(b)).

$$h = h_0 exp(kt) + \frac{\alpha P(exp(kt) - 1)}{kn} \tag{4}$$

Here, h, h_0, P and t indicate the groundwater level, the initial value of the groundwater level, the precipitation obtained at discrete intervals and the time, respectively, and k, α and n are the rate coefficient to groundwater discharge, the ratio of recharge to precipitation and the fillable porosity in the ground, respectively. h, P and t are observations, and we estimated α/n and k. The groundwater level data (h) and the precipitation data (P) for one year before the earthquake in 2016 were used to determine α/n and k. These data were then used to calculate the

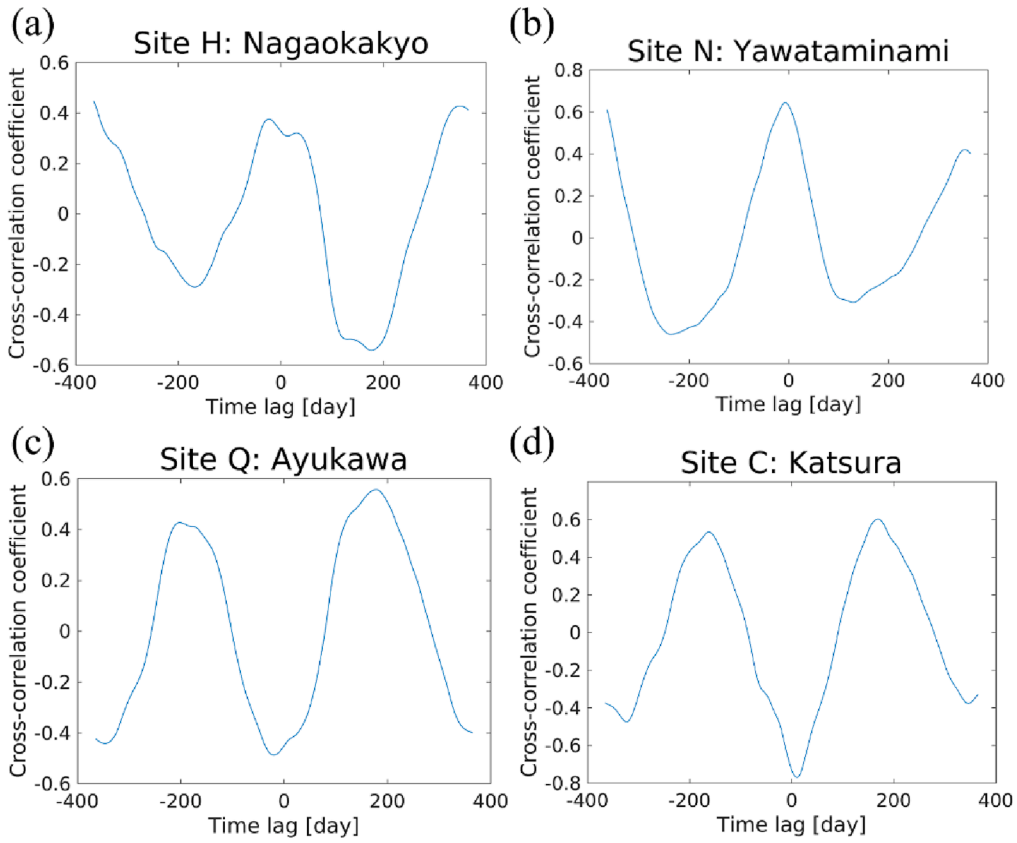

Fig. 7. Cross-correlation coefficients between the surface displacements and the groundwater level changes within a one-year time lag τ during the periods before and after the 2018 northern Osaka earthquake. The time lag τ indicates the time difference between two sets of data when calculating the cross-correlation coefficient.

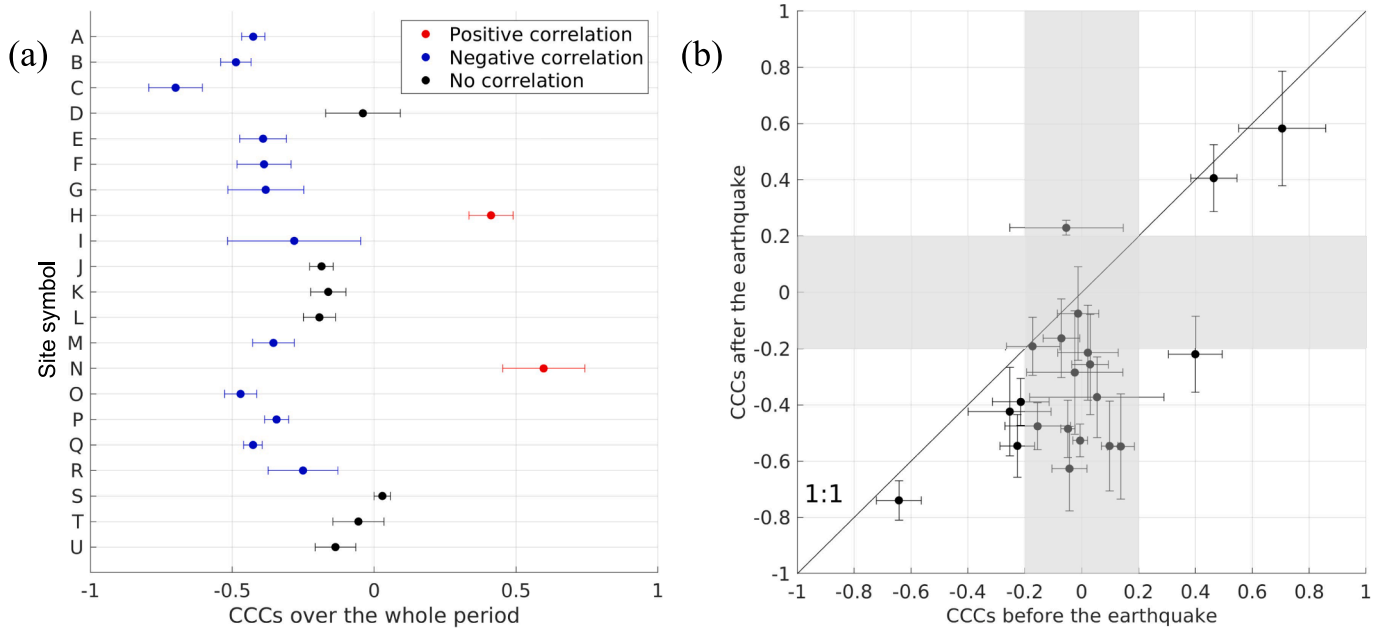

Fig. 8. (a) Comparison of the cross-correlation coefficients (CCCs) between the surface displacements and the groundwater level changes from 2017 to 2020. The time lag to calculate the coefficient was set to zero days. The solid circles and error bars indicate the average and standard deviations of the CCCs between the surface displacements obtained from the six conditions of the PSInSAR analysis and the groundwater level changes, respectively. (b) Comparison of the CCCs before and after the 2018 northern Osaka earthquake. The straight line indicates a 1:1 relationship.

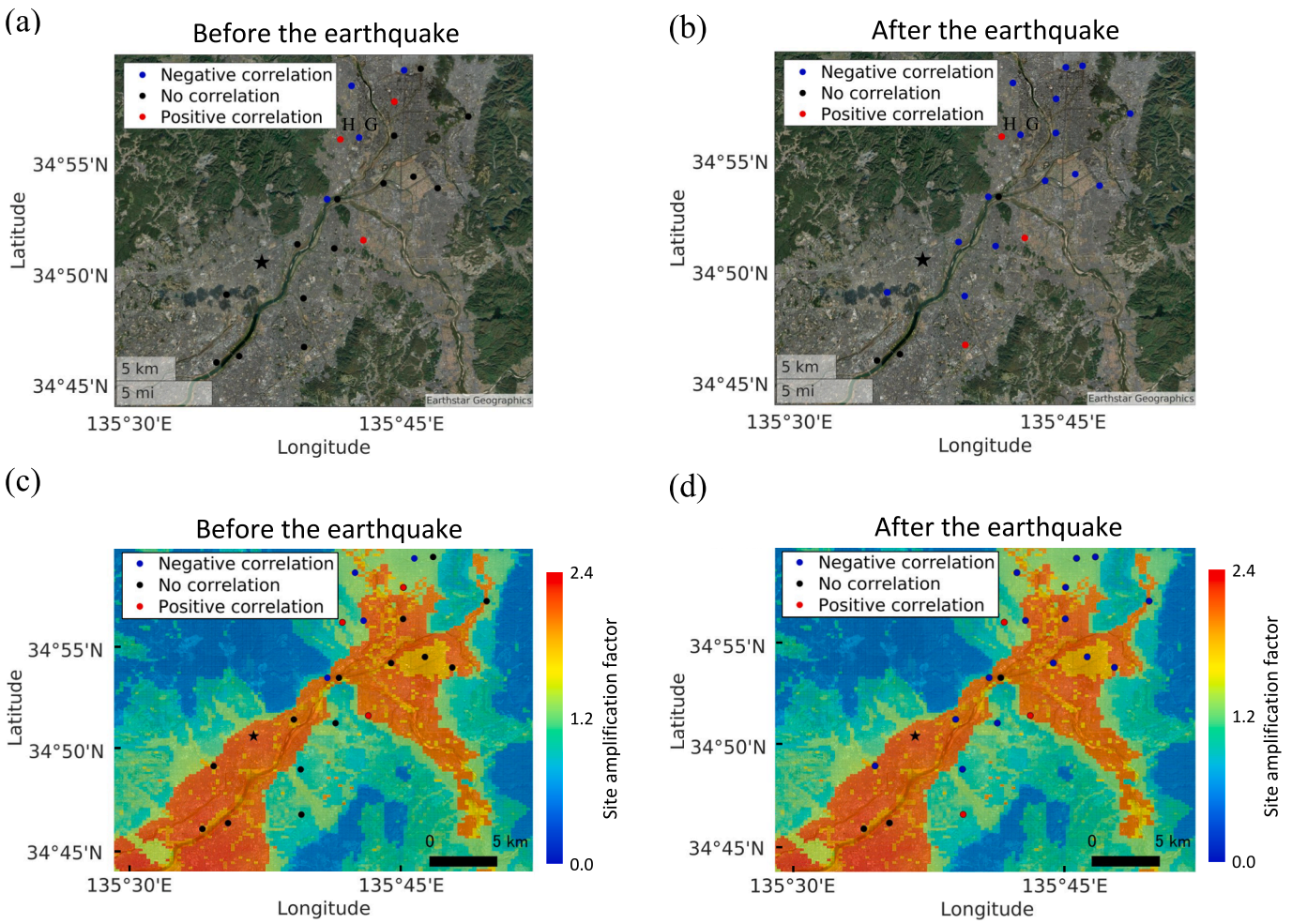

Fig. 9. Distribution of CCCs (a) before and (b) after the earthquake for all the groundwater level observation sites in the Osaka and Kyoto area (see Table 2 for definitions of H and G). The black star indicates the epicentre of the earthquake. Overlaid map of the site amplification factor (National Research Institute for Earth Science and Disaster Resilience, 2019) and distribution of the correlation changes (c) before and (d) after the earthquake. The site amplification factor map was calculated from the average shear-wave velocity in the upper 30 m (AVS30). The site amplification factor assumes the maximum velocity amplification from the engineering base surface (Vs = 400 m/s) to the ground surface.

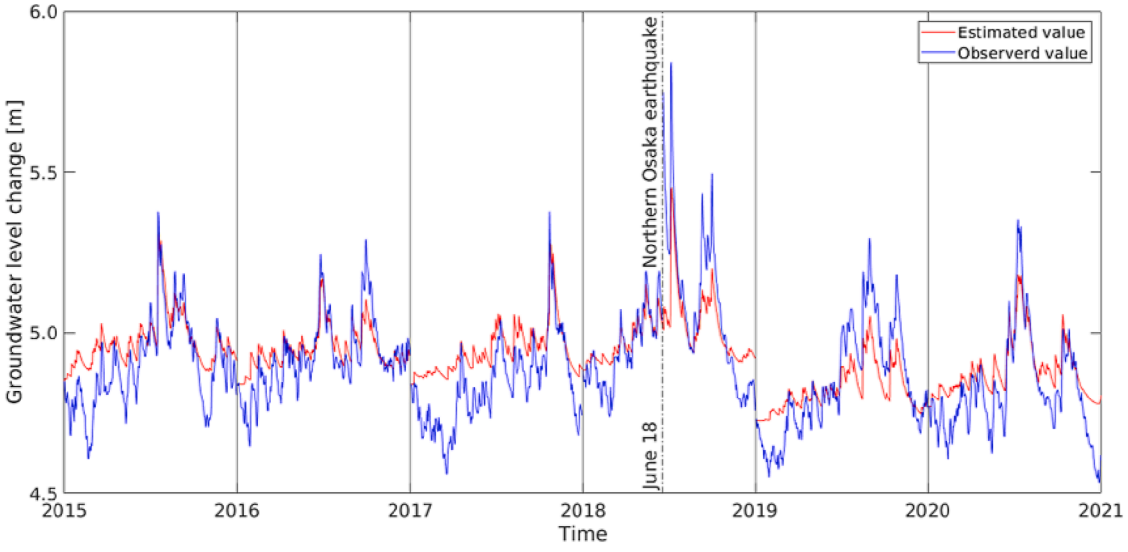

Fig. 10. Comparison of the groundwater level change estimated using the numerical algorithm (Park and Parker, 2008) and the observed groundwater level change.

estimated groundwater level for each year from 2015 to 2020 (Fig. 10). The groundwater level on January 1 of each year was used as the initial value for the calculation. The fmincon algorithm in MATLAB was used to solve the nonlinear optimization problem.

The estimated values of the groundwater level are in good agreement with the measured values both in their changing trends and at their peaks, especially prior to the earthquake, suggesting a good representation of the increase in the groundwater level as a result of precipitation during the examined period (Fig. 10). Conversely, the measured values frequently exceeded the estimated values after the earthquake. This result suggests that the amount of groundwater per unit of precipitation increased as a result of the earthquake, for example, the permeability may have increased as a result of the earthquake, as suggested in previous studies (Liu et al., 2018). Note that the estimated local minimum peak does not agree with the measured values. This mismatch occurs because Eq. (4) does not consider the drainage from the initial value.

The estimated parameters in Eq. (4) were $\alpha/n = 1.5 \times 10^{-3}$ and $k = -5.9 \times 10^{-2}$ T^{-1} before the earthquake and $\alpha/n = 1.5 \times 10^{-3}$ and $k = -2.7 \times 10^{-2}$ T^{-1} after the earthquake. Because k is proportional to the inverse of n, this implies that n and αbecame twice as large after the earthquake. This result suggests that the earthquake increased the porosity and recharge rate of the groundwater and therefore increased the amount of groundwater.

4.2. Change in the pseudoelastic constant before and after the earthquake

The enhancement of the negative correlation between the surface displacements and the groundwater level changes also implies that the susceptibility of the surface displacements per unit change in the hydraulic head was likely altered by the earthquake. To investigate this phenomenon in more detail, we calculated the ratio of the daily groundwater level changes to the daily surface displacements and compared these ratios before and after the earthquake. When the groundwater level changes and the surface displacements are positively correlated, their ratio is known as the skeletal storage coefficient (Chen et al., 2017; Ishitsuka and Tsuji, 2019). However, this does not hold when the correlation is negative. Instead, we treat the constant ratio as a pseudoelastic constant because, according to Lu et al. (2020), a negative correlation NC indicates that the surface displacements are caused primarily by the water mass load. Conversely, a positive value of the pseudoelastic constant indicates that the surface displacements are caused primarily by the pore water pressure. The absolute value of the pseudoelastic constant indicates the degree of susceptibility to surface displacements caused by groundwater level changes. When the pseudoelastic constant becomes small, a slight increase in the pore water pressure or water mass load will cause surface displacements. In this study, we estimated the pseudoelastic constants by dividing the surface displacements and the groundwater level change data into the periods before and after the earthquake. Specifically, the least squares method was applied to the data before and after the earthquake to obtain the slope of the line showing the inverse of the pseudoelastic constant.

The calculated pseudoelastic constant at the groundwater level observation site Q is shown in Fig. 11(a). At this site, the pseudoelastic constant was negative, suggesting that the ground displacements were caused by the water mass load. The estimated pseudoelastic constants before and after the earthquake at all observation sites are shown in Fig. 11(b). At most sites, the pseudoelastic constants became smaller after the earthquake (see Fig. S5). The negative change in the pseudoelastic constant supports the conjecture that an earthquake-induced increase in the permeability and porosity (Elkhoury et al., 2006; Manga et al., 2012) resulted in a modification of the elastic properties of the aquifer. The exception is sites N and T, Yahataminami and Shimeno, where the pseudoelastic constant was positive and the pseudoelastic constant became larger after the earthquake (Fig. 11(b)). This increase in the constant can be explained by an increase in the pore water pressure as opposed to an increase in the water mass load.

4.3. Possible aquifer dynamical models

As briefly introduced in Section 1, Lu et al. (2020) proposed that the seasonal surface displacements depend on the balance between the pore pressure and the water mass load in an aquifer. When the influence of the mass load exceeds that of the pore pressure increase, the ground surface subsides even when the groundwater level increases (i.e., negative correlation). Based on this model and our observations of permeability and porosity increases after the 2018 earthquake, we surmise that the increase in negative correlations after the earthquake can be attributed to the rise in the groundwater levels resulting from the increase in the groundwater volume and the associated increase in the water mass load. This interpretation entails a new conceptual aquifer

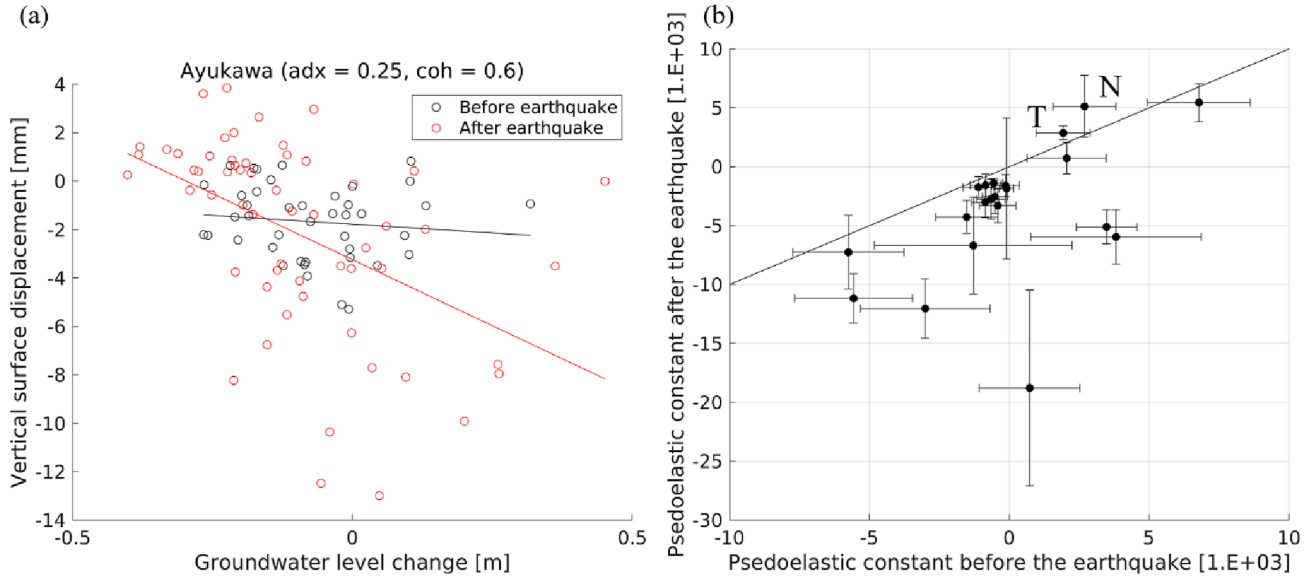

Fig. 11. (a) Change in the pseudoelastic constants before and after the earthquake at site Q: Ayukawa. The slope of the straight line is the inverse of the pseudoelastic constant. (b) Variation in the pseudoelastic constants before and after the earthquake. The straight line represents a 1:1 correlation. The black circles and error bars indicate the average values and the standard deviations, respectively.

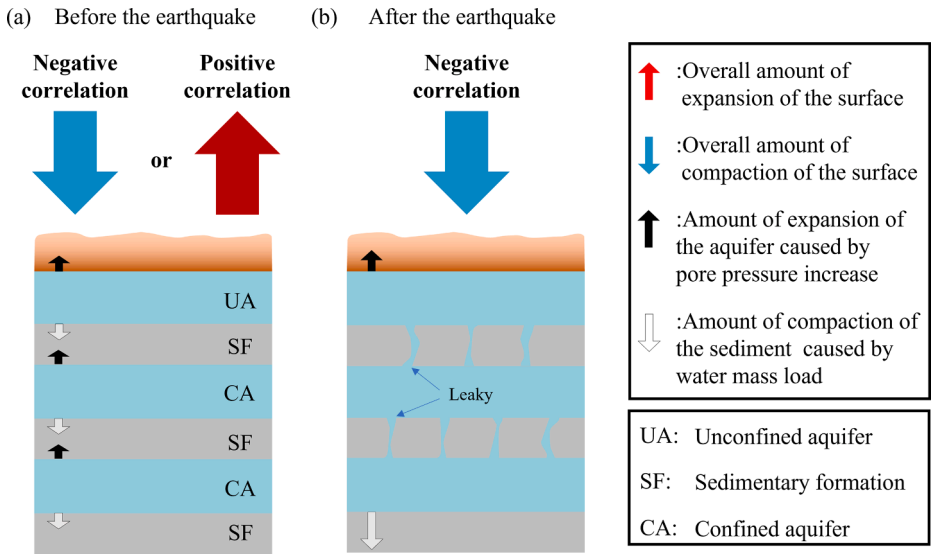

Fig. 12. Dynamical model of aquifers representing the mechanism of seasonal component correlations between the surface displacement and the groundwater level changes assuming an increase in groundwater level (a) before and (b) after an earthquake.

dynamical model in which negative correlation increases resulting from an earthquake are simplified and explained (Fig. 12). Fig. 12 illustrates the case of an increase in groundwater level. Fig. 12(a) shows the ordinal state of an aquifer system in which the aquifer and aquitard interbed each other. Seasonal groundwater level changes usually occur in shallow aquifers because of seasonal precipitation changes (Fig. 5). In Fig. 12(b) after the earthquake, as discussed in Sections 4.1 and 4.2, the lower confined aquifer is connected to the upper confined aquifer as the permeability or porosity increases because of seismic vibrations (i.e., the aquifer structure changes to a leaky model). Subsequently, the effect of the pore pressure on the surface displacement decreases and the effect of the water mass load increases, resulting in the appearance or increase of negative correlations. Note that the correlation is determined by the dynamical balance of the system as a whole; therefore, unless there is a connection between the aquifers because of an event such as an earthquake, the correlation is expected to be relatively small.

5. Conclusions

In this study, by applying DInSAR and PSInSAR analyses to the Osaka and Kyoto areas, Japan, where the 2018 northern Osaka earthquake occurred, we found that Mw 6-class earthquakes can influence aquifer property changes over a wide area. This finding was based on the conceptual aquifer dynamical model of Lu et al. (2020) and our results, using CCCs, that the seasonal surface displacements were correlated with the groundwater level changes. To the best of our knowledge, this is the first time that it has been confirmed that Mw 6-class earthquakes affect not only the linear correlation between surface displacements and the groundwater level changes but also the seasonal component correlation. This change in the correlation is explained by changes in the aquifer properties (i.e., porosity, permeability and the recharge rate of the groundwater) induced by the earthquake. Using satellite data, we identified changes in the aquifer properties over a wide area after the earthquake. That is, we temporally and spatially captured an important natural phenomenon in which aquifer properties change because of an earthquake. The results were validated from multiple perspectives, including pre- and post-earthquake groundwater responses, aquifer properties, pseudoelastic constants, changes in the spatial properties and possible aquifer models. Explanations of the overall mechanisms of the surface and subsurface after earthquakes will contribute to obtaining useful information for groundwater level monitoring and subsurface resource development.

Declaration of Competing Interest

The authors declare that they have no known competing financial interests or personal relationships that could have appeared to influence the work reported in this paper.

Data availability

I have shared the link to my data.

Acknowledgments

We would like to express our gratitude to the European Space Agency (ESA) for providing the Sentinel-1A SAR data, the Water Quality Database of the Ministry of Land, Infrastructure, Transport and Tourism (MLIT), Japan for providing the groundwater level and observation sites data, and National Research Institute for Earth Science and Disaster Resilience for providing site amplification factor map in accordance with their open data policy. We also would like to thank the Japanese Meteorological Agency for providing precipitation data. We thank Martha Evonuk, PhD, from Edanz (https://jp.edanz.com/ac), for editing a draft of this manuscript. This work was partially supported by JSPS KAKENHI Grant Number JP22J14212.

Appendix A. Supplementary material

The SLC data for InSAR analysis and groundwater level data are available through https://zenodo.org/record/6644133#.YrVRrnbP2Uk (https://doi.org/10.5281/zenodo.6644133). The authors would like to thank the European Space Agency (ESA) (https://search.asf.alaska.edu/#/), and the Water information System, Ministry of Land, Infrastructure, Transport and Tourism (https://www1.river.go.jp/). Supplementary data to this article can be found online at https://doi.org/10.1016/j.jag.2023.103394.

References

Castellazzi, P., Garfias, J., Martel, R., Brouard, C., Rivera, A., 2017. InSAR to support sustainable urbanization over compacting aquifers: The case of Toluca Valley, Mexico. Int. J. Appl. Earth Obs. Geoinf. 63, 33–44. https://doi:10.1016/j.jag.2017.06.011.

Chaussard, E., Wdowinski, S., Cabral-Cano, E., Amelung, F., 2014. Land subsidence in central Mexico detected by ALOS InSAR time-series, *Remote Sens.* Environ. 140, 94–106. https://doi:10.1016/j.rse.2013.08.038.

Chen, J., Knight, R., Zebker, H.A., 2017. The temporal and spatial variability of the confined aquifer head and storage properties in the San Luis valley, Colorado inferred from multiple InSAR missions. Water Resour. Res. 53, 9708–9720. https://doi:10.1002/2017wr020881.

Elkhoury, J.E., Brodsky, E.E., Agnew, D.C., 2006. Seismic waves increase permeability. Nature 441, 1135–1138. https://doi:10.1038/nature04798.

Ferretti, A., Prati, C., Rocca, F., 2000. Nonlinear subsidence rate estimation using permanent scatterers in differential SAR interferometry. IEEE Trans. Geosci. Remote Sens. 38, 2202–2212. https://doi:10.1109/36.868878.

Ferretti, A., Prati, C., Rocca, F., 2001. Permanent scatterers in SAR interferometry. IEEE Trans. Geosci. Remote Sens. 39, 8–20. https://doi:10.1109/36.898661.

Fialko, Y., 2004. Evidence of fluid-filled upper crust from observations of postseismic deformation due to the 1992 Mw7.3 Landers earthquake. J. Geophys. Res. 109, B08401. https://doi:10.1029/2004jb002985.

Fielding, E.J., Lundgren, P.R., Bürgmann, R., Funning, G.J., 2009. Shallow fault-zone dilatancy recovery after the 2003 Bam earthquake in Iran. Nature 458, 64–68. https://doi-org.kyoto-u.idm.oclc.org/10.1038/nature07817.

Fujiwara, S., Nishimura, T., Murakami, M., Nakagawa, H., Tobita, M., Rosen, P.A., 2000. 2.5-D surface deformation of M6.1 earthquake near Mt Iwate detected by SAR interferometry. Geophys. Res. Lett. 27, 2049–2052. https://doi:10.1029/1999gl011291.

Hashimoto, M., 2016. Observation of ground deformation in the Osaka and Kanto plains with ALOS-2/PALSAR-2, 2016 IEEE International Geoscience and Remote Sensing Symposium (IGARSS), 3855–3858. https://doi:10.1109/IGARSS.2016.7730000.

Hatanaka, Y., Iizuka, T., Sawada, M., Yamagiwa, A., Kikuta, Y., Johnson, J.M., Rocken, C., 2003. Improvement of the analysis strategy of GEONET. Bull. GSI 49, 11–37.

Heki, K., Arief, S., 2022. Crustal response to heavy rains in Southwest Japan 2017–2020. Earth Planet. Sci. Lett. 578, 117325. https://doi:10.1016/j.epsl.2021.117325.

Hirata, N., Kimura, R., 2018. The Earthquake in Ōsaka-Fu Hokubu on 18 June 2018 and its Ensuing Disaster. J. Disaster Res. 13 (4), 813–816.

Hooper, A., Bekaert, D., Spaans, K., Arıkan, M., 2012. Recent advances in SAR interferometry time series analysis for measuring crustal deformation. Tectonophysics 514–517, 1–13. https://doi:10.1016/j.tecto.2011.10.013.

Hooper, A., Zebker, H.A., 2007. Phase unwrapping in three dimensions with application to InSAR time series. J. Opt. Soc. Am. A Opt. Image Sci. Vis. 24, 2737–2747. https://doi:10.1364/josaa.24.002737.

Hosono, T., Yamada, C., Shibata, T., Tawara, Y., Wang, C.-Y., Manga, M., Rahman, A.T. M.S., Shimada, J., 2019. Coseismic groundwater drawdown along crustal ruptures during the 2016 Mw7.0 Kumamoto earthquake. Water Resour. Res. 55, 5891–5903. https://doi:10.1029/2019WR024871.

Ishitsuka, K., Tsuji, T., 2019. Mapping Surface Displacements and Aquifer Characteristics Around the Kumamoto Plain, Japan, Using Persistent Scatterer Interferometry, IGARSS 2019 - 2019 IEEE International Geoscience and Remote Sensing Symposium, 9654–9657. https://doi:10.1109/IGARSS.2019.8897893.

Ishitsuka, K., Tsuji, T., Matsuoka, T., 2016. Surface displacement around the Ezu Lake and the Suizeni area associated with the 2016 Kumamoto earthquake, J. Remote Sens. Soc. Japan, 36, 218-222 (in Japanese). https://doi.org/10.11440/rssj.36.218.

Ishitsuka, K., Fukushima, Y.o., Tsuji, T., Yamada, Y., Matsuoka, T., Giao, P.H., 2014. Natural surface rebound of the Bangkok plain and aquifer characterization by persistent scatterer interferometry. Geochem. Geophys. Geosyst 15 (4), 965–974. https://doi.org/10.1002/2013GC005154.

Ishitsuka, K., Matsuoka, T., Nishimura, T., Tsuji, T., ElGharbawi, T., 2017. Ground uplift related to permeability enhancement following the 2011 Tohoku earthquake in the Kanto Plain, Japan. Earth Planets Space 69, 1–10. https://doi:10.1186/s40623-017-0666-7.

Ishitsuka, K., Tsuji, T., Lin, W., Kagabu, M., Shimada, J., 2020. Seasonal and transient surface displacements in the Kumamoto area, Japan, associated with the 2016 Kumamoto earthquake: implications for seismic-induced groundwater level change. Earth Planets Space 72, 144. https://doi:10.1186/s40623-020-01275-2.

Jónsson, S., Segall, P., Pedersen, R., Björnsson, G., 2003. Post-earthquake ground movements correlated to pore-pressure transients. Nature 424, 179–183. https://doi:10.1038/nature01776.

Kampes, B.M., 2006. Radar Interferometry. Springer, Netherlands https://doi:10.1007/978-1-4020-4723-7.

Liu, C.-Y., Chia, Y., Chuang, P.-Y., Chiu, Y.-C., Tseng, T.-L., 2018. Impacts of hydrogeological characteristics on groundwater-level changes induced by earthquakes. Hydrogeol. J. 26 (2), 451–465. https://doi.org/10.1007/s10040-017-1684-z.

Lu, C.-Y., Hu, J.-C., Chan, Y.-C., Su, Y.-F., Chang, C.-H., 2020. The Relationship between Surface Displacement and Groundwater Level Change and Its Hydrogeological Implications in an Alluvial Fan: Case Study of the Choshui River, Taiwan. Remote Sens. 12, 3315. https://doi:10.3390/rs12203315.

Manga, M., Beresnev, I., Brodsky, E.E., Elkhoury, J.E., Elsworth, D., Ingebritsen, S.E., Mays, D.C., et al., 2012. Changes in permeability caused by transient stresses: Field observations, experiments, and mechanisms. Rev. Geophys. 50, RG2004. https://doi:10.1029/2011rg000382.

Massonnet, D., Feigl, K.L., 1998. Radar interferometry and its application to changes in the Earth's surface. Rev. Geophys. 36 (4), 441–500. https://doi.org/10.1029/97RG03139.

Morishita, Y., 2021. Nationwide urban ground deformation monitoring in Japan using Sentinel-1 LiCSAR products and LiCSBAS. Progr. Earth Planet. Sci. 8, 6. https://doi:10.1186/s40645-020-00402-7.

Moro, M., Saroli, M., Stramondo, S., Bignami, C., Albano, M., Falcucci, E., Gori, S., Doglioni, C., Polcari, M., Tallini, M., Macerola, L., Novali, F., Costantini, M., Malvarosa, F., Wegmüller, U., 2017. New insights into earthquake precursors from InSAR. Sci. Rep. 7 (1). https://doi.org/10.1038/s41598-017-12058-3.

Mourad, M., Tsuji, T., Ikeda, T., Ishitsuka, K., Senna, S., Ide, K., 2021. Mapping Aquifer Storage Properties Using S-Wave Velocity and InSAR-Derived Surface Displacement in the Kumamoto Area, Southwest Japan. Remote Sens. 13, 4391. https://doi:10.3390/rs13214391.

National Research Institute for Earth Science and Disaster Resilience, J-SHIS, http://www.j-shis.bosai.go.jp/map/, 2019, https://doi.org/10.17598/nied.0010.

Neely, W.R., Borsa, A.A., Burney, J.A., Levy, M.C., Silverii, F., Sneed, M., 2021. Characterization of groundwater recharge and flow in California's San Joaquin Valley from InSAR-observed surface deformation, Water Resour. Res., 57, e2020WR028451. https://doi:10.1029/2020WR028451.

Normand, J.C.L., Heggy, E., 2015. InSAR assessment of surface deformations in urban coastal terrains associated with groundwater dynamics. IEEE Trans. Geosci. Remote Sens. 53, 6356–6371. https://doi:10.1109/TGRS.2015.2437368.

Park, E., Parker, J.C., 2008. A simple model for water table fluctuations in response to precipitation. J. Hydrol. 356, 344–349. https://doi:10.1016/j.jhydrol.2008.04.022.

Shintani, T., Masuda, H., Nemoto, T., Ikawa, R., Marui, A., Tanimizu, M., Ishikawa, T., 2022. Three-dimensional structure and sources of groundwater masses beneath the Osaka Plain, Southwest Japan. J. Hydrol.: Regional Stud. 43, 101193. https://doi:10.1016/j.ejrh.2022.101193.

Taniguchi, M., Uemura, T., 2005. Effects of urbanization and groundwater flow on the subsurface temperature in Osaka, Japan. Phys. Earth Planet. Inter. 152, 305–313. https://doi:10.1016/j.pepi.2005.04.006.

Tokunaga, T., 1999. Estimating Permeability Change and Specific Yield from Earthquake-induced Hydrological Changes: an Example from Kobe Earthquake. J. Japan Soc. Eng. Geol. 40 (2), 99–106 (in Japanese). https://doi.org/10.5110/jjseg.40.99.

Wald, D.J., Heaton, T.H., 1994. Spatial and temporal distribution of slip for the 1992 Landers, California, earthquake. Bull. Seismol. Soc. Am. 84, 668–691. https://doi:10.1785/BSSA0840030668.

Wang, S., Xu, W., Xu, C., Yin, Z., Bürgmann, R., Liu, L., Jiang, G., 2019. Changes in groundwater level possibly encourage shallow earthquakes in central Australia: The 2016 Petermann ranges earthquake. Geophys. Res. Lett. 46, 3189–3198. https://doi:10.1029/2018gl080510.

Wegnüller, U., Werner, C., Strozzi, T., Wiesmann, A., Frey, O., Santoro, M., 2016. Sentinel-1 support in the GAMMA software. Procedia Comput. Sci. 100, 1305–1312. In: https://doi:10.1016/j.procs.2016.09.246.

Werner, Wegmüller & Strozzi., 2000. Gamma SAR and interferometric processing software, Proc. Estonian Acad. Sci. Biol. Ecol., Cite. Retrieved from https://citeseerx.ist.psu.edu/viewdoc/download?doi=10.1.1.201.7836&rep=rep1&type=pdf.

Yoneda, M., Morisawa, S., Takine, N., Fukuhara, S., Takeuchi, H., Hirano, T., Takahashi, H., Inoue, Y., 2001. Groundwater Deterioration Caused by Induced Recharge: Field Survey and Verification of the Deterioration Mechanism by Stochastic Numerical Simulation. Water Air Soil Pollut 127, 125–156. https://doi.org/10.1023/A:1005251716246.

Zhan, W., Heki, K., Arief, S., Yoshida, M., 2021. Topographic amplification of crustal subsidence by the rainwater load of the 2019 typhoon hagibis in Japan, J. Geophys. Res. [Solid Earth], 126, e2021JB021845. https://doi:10.1029/2021jb021845.

Zhou, C., Gong, H., Chen, B., Gao, M., Cao, Q., Cao, J., Duan, L.i., Zuo, J., Shi, M., 2020. Land Subsidence Response to Different Land Use Types and Water Resource Utilization in Beijing-Tianjin-Hebei, China. Remote Sens 12 (3), 457. https://doi.org/10.3390/rs12030457.